# Chapter 1

# Quasar spectra

## 1.1 Composite quasar spectra

In the ealy 1970s, Davidson (1972) promoted the notion of a composite spectrum, purporting the utility of its application for studying the nature of the quasar structure— "If all of the major emission lines between 1000 and 7000 Å are to considered in a model, it is neccessary to adopt a composite *typical* spectrum." Davidson's "composite" quasar spectrum was based upon normalizing the relative intensities of ten emission lines measured for eleven quasars, "adapted from estimates by several observers". Who these observers are and how they estimated the relative intensities is lost to history. Davidson's data matrix was sparse. Later in the decade, a statistical examination of the properties of quasar emission line strengths was undertaken by Chan & Burbidge (1975) using 160 quasar spectra. Their "composite average spectrum" was also a simple list of the averaged relative emission line intensities. These studies were, in a sense, the first step in forming what is known as a true composite spectrum.

Constructing a composite spectrum requires several important objectively defined steps. The steps are roughly as follows.

1. Accurately determined the systemic, or emission redshift for each individual quasar in a the full sample.

2. Clean, or mask bad pixels in each individual quasar in the full sample. Often this requires interpolating across or masking out fixed pattern noise, predominant telluric features such as the A and B bands, and cosmic rays.

3. De–redshift each individual quasar spectrum into the rest–frame by scaling the observed wavelength, $\lambda_o$, using $\lambda = \lambda_o/(1 + z_{em})$.

4. If not preserving the spectral energy distribution, continuum normalize the continuum source of each individual spectrum, being careful to prserve the emission lines. If preserving the spectral energy distribution, correct the de–redshifting by scaling the observed flux using $f_\lambda = f_{\lambda_o}(1 + z_{em})$, and then normalize the individual spectra at a arbitrarily chosen wavelength (preferable where the continnum is featureless).

5. If desired, rebin the wavelengths to a linear dispersion (wavelength per pixel) that is similar to the dispersion of the spectra for each individual quasar. This process can simplify the co–adding step; if the spectra are not interpolated prior to co–addition, then they may require interpolation during the co–addition step. (Here it is assumed that not every spectrum has identical wavelength versus pixel calibrations).

6. From the full sample of quasars, define subsamples. For example, most composites spectra omit spectra exhibiting broad $\sim$ 5000 km sec$^{-1}$ absorption lines. Also, the sample may be divided by other properties (if available), such as radio and/or X–ray luminosity and/or variablility, redshift range, radio spectral index, optical to X–ray index, presence of narrow absorption lines with $z_{abs} \sim z_{em}$, etc.

7. Employing an objectively defined algorithm, co–add the spectra in the selected subsample to create the resulting composite spectrum.

Check this too: (Forster *et al.*, 2001)

Determining the emission redshifts of each quasar is not an naively straight forward process. One of the issues at hand is that the rest wavelength positions of the emission lines in quasars are known to be shifted from their laboratory values. One method for determining the systematic, or emission, redshifts of the quasars is to measure the centroid of the narrow, forbidden O III $\lambda$5007 emission line McIntosh*et al.* (e.g., 1999); Vanden Burk *et al.* (e.g., 2001, and references therein). Using this technique, McIntosh*et al.* (1999) find the non–resonance H$\beta$ line is systematically shifted $\simeq +520$ km sec$^{-1}$, whereas the broad emission lines from high–ionization transitions are blueshifted over the range $-550$ to $-1050$ km sec$^{-1}$. They suggest that the Mg II $\lambda$2800 emission line may also served as a good measure of the emission redshift, since it is shifted within $\pm$50 km sec$^{-1}$ of the O III line.

The two most common methods for co–adding the individual spectra are the arithmetic mean and the geometric mean. Each has its advantage for studying the two prominant intrinsic features of quasar spectra– the absolute and relative intensities and profile shapes of the broad, narrow, and forbidden emission lines, and the spectra energy distribution of the continuum source.

From absolute scanner photometry in the late 1960s and early 1970s, it was quickly realized that the spectral energy distribution of the rest–frame optical and ultraviolet continuum is characterized by a power law,

$$f_\nu \, d\nu \propto \nu^{\alpha_\nu} \, d\nu, \tag{1.1}$$

where $f_\nu$ is the frequency monochromatic flux [erg s$^{-1}$ cm$^{-2}$ Hz$^{-1}$] with an average spectral index $\alpha_\nu = -1$ over the range $-2 \leq \alpha_\nu \leq 0$ (Oke, 1966; Wampler, 1967; Oke, Neugebauer, & Becklin, 1970). With the advent of multichannel detectors, Baldwin (1975) found that that a single power–law spectal index does not, in general, fit the continuum; He reported a change in slope in the rest–frame wavelength region of 3000–4000 Å. In modern CCD data, this change in slope is now found to lie between the H$\beta$ and H$\alpha$ emission lines and is dubbed the "near–infrared inflection" (e.g. Vanden Burk *et al.*, 2001).

Since spectra are often presented as a function of wavelength, the continuum spectral energy distribution of quasars is often expressed as $f_\lambda$, the wavelength monochromatic flux [erg s$^{-1}$ cm$^{-2}$ Å$^{-1}$]. From $c = \lambda\nu$ and energy conservation, $f_\lambda d\lambda = f_\nu d\nu$, we have

$$f_\lambda \, d\lambda \propto \left(\frac{1}{\lambda}\right)^{\alpha_\nu} \frac{d\lambda}{\lambda^2} \propto \lambda^{-(\alpha_\nu+2)} \, d\lambda, \tag{1.2}$$

in terms of the frequency power–law spectral index.

The geometric mean naturally yields a composite spectrum in which the resulting power–law spectral energy distribution of the composite is the arithmetic mean of the spectral energy distributions of the individual contributing quasars. Assuming the observed flux, $f_\lambda$, or flux calibrated counts, $I_\lambda$, have been normalized at a selected wavelength, then the geometric mean of the counts at wavelength $\lambda$ is

$$\langle I_\lambda \rangle = \left\{ \prod_{i=1}^{N} [I_\lambda]_i \right\}^{1/N} \tag{1.3}$$

where the product is over the number of quasars in the sample for which measured counts are available at wavelength $\lambda$. Employing Eq. 1.2 in terms of calibrated counts, we have

$$\langle I_\lambda \rangle = \left\{ \prod_{i=1}^{N} C_i \lambda_i^{-(\alpha_\nu+2)} \right\}^{1/N} = \langle C \rangle \, \lambda^{-(\langle\alpha_\nu\rangle+2)}, \tag{1.4}$$

where $\langle\alpha_\nu\rangle$ is the arithmetic mean of the spectral index and $\langle C \rangle$ is the geometric mean of the normalization applied to each spectrum,

$$\langle \alpha_\nu \rangle = \frac{1}{N} \sum_{i=1}^{N} [\alpha_\nu]_i \,, \qquad \langle C \rangle = \left\{ \prod_{i=1}^{N} C_i \right\}^{1/N} . \tag{1.5}$$

Relative to the local continuum, mean integrated intensities, profile shapes, and cetnroids of the broad, narrow, and forbidden emission lines can be measured using the arithmetic mean, since it provides the independent mean in each wavelength bin. Since the arithmetic mean does not yield the mean spectral energy distribution, it is common to normalize the individual spectra contributing

to the composite spectrum, i.e., to fit a smooth function to the each quasar continuum, $I^0_\lambda$, and divide this function into the observed counts, yielding, $I_\lambda/I^0_\lambda$. The unweighted arithmetic mean is then computed according to

$$\left\langle I_\lambda/I^0_\lambda \right\rangle = \frac{1}{N}\sum_{i=1}^{N}\left[I_\lambda/I^0_\lambda\right]_i , \tag{1.6}$$

where the sum is over the number of quasars in the sample for which measured counts are available at wavelength $\lambda$.

The weighted arithmetic mean

$$\left\langle I_\lambda/I^0_\lambda \right\rangle = \frac{1}{W}\sum_{i=1}^{N} w_i \left[I_\lambda/I^0_\lambda\right]_i , \tag{1.7}$$

the weighted geometric mean

$$\left\langle I_\lambda/I^0_\lambda \right\rangle = \left\{\prod_{i=1}^{N}\left[C_i\lambda_i^{-(\alpha_\nu+2)}\right]^{w_i}\right\}^{1/W} = \exp\left\{\frac{1}{W}\sum_{i=1}^{N} w_i \ln\left[I_\lambda/I^0_\lambda\right]_i\right\}, \tag{1.8}$$

where $W = \sum_{i=1}^{N} w_i$, and $w_i = 1/\sigma_i$, where $\sigma_i$ is the uncertainty in $[I_\lambda/I^0_\lambda]_i$ or $[I_\lambda]_i$.

The composite spectrum from the data obtained with the 2dF and 6dF QSO Redshift Surveys (Croom *et al.*, 2002)[1] is presented in Figure 1.1. Shifted into rest frame of the quasar, the wavelength range of this composite spectrum covers 900–7000 Å. The emission lines most commonly identified in quasar spectra over this wavelength range are labeled. The Croom *et al.* (2002) spectrum is

Because the range of observed wavelengths is fixed for the survey, and because there is a distribution of quasars redshifts in the sample, there is not an equal number of quasars at each rest–fram wavelength. Thus, the signal–to–noise ratio is not constant with wavelength in the compisite spectrum.

*HST*+SDSS composite spectrum[2]

FUSE composite spectrum[3]

For both broad and narrow emission lines, Vanden Burk *et al.* (2001, see their Figure 9) find an anti–correlation between ionization potential of the species and the magnitude of the velocity shift; low ionization potential lines (less than 25 eV) have offset velocities ranging from consistent with systematic to +300 km sec$^{-1}$, whereas higher ionization potential lines (between 45 to 65 eV) have velocity offsets in the range −200 to −600 km sec$^{-1}$.

A composite spectrum is shown in Figure 1.1. and the HST+SDSS Figure 1.2.

$f_\nu \propto \nu^{\alpha_\nu}$

$\alpha_\nu = -1.76$ for wavelengths less than 1300 Å

[1] *http://www.2dfquasar.org/Spec_Cat/composites/composite.html*

[2] *http://www.pha.jhu.edu/∼rt19/composite/*

[3] *http://archive.stsci.edu/prepds/composite_quasar/*

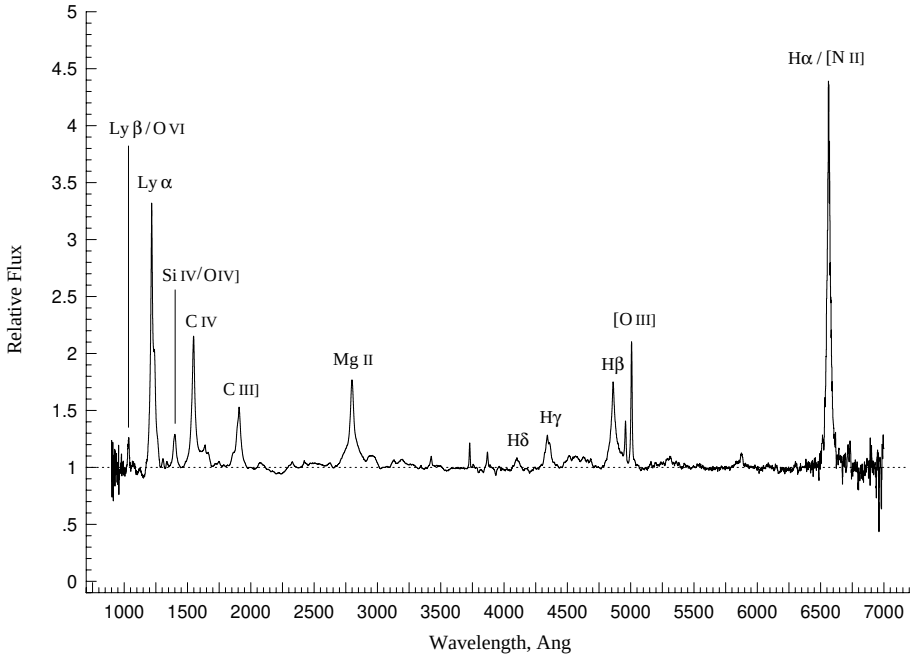


Figure 1.1: The composite quasar spectrum (median) constructed by Croom *et al.* (2002) using 22,000 spectra from the 2dF and 6dF QSO Redshift Surveys. The spectrum covers the rest–frame wavelength range 900–7000 Å. Major emission lines are labeled. [Data obtained from the 2QZ website.]

$\alpha_\nu = -0.45$ for wavelengths over the range 1300–4670 Å

$\alpha_\nu = -1.65$ for wavelengths greater than 4670 Å

$\alpha_\lambda = -(\alpha_\nu + 2)$

An excellent illustration of the FeII emission above the continuum Figure 2 of Boyle (1990)

### 1.1.1 emission properties

## 1.2 The broad emission line (BEL) region

correlation of line widths between BELs and BALs (Lee & Turnsheck 1995). The WHIM wind can [pressure confine coolr higher density clouds.

(Murray & Chiang, 1998)

column densities of order $10^22$ with no upper limit (**?**) [from Elvis]

see paper by Baldwin 1997 (on Mac) - Table 1. radio properties Green 98 has X-ray properties

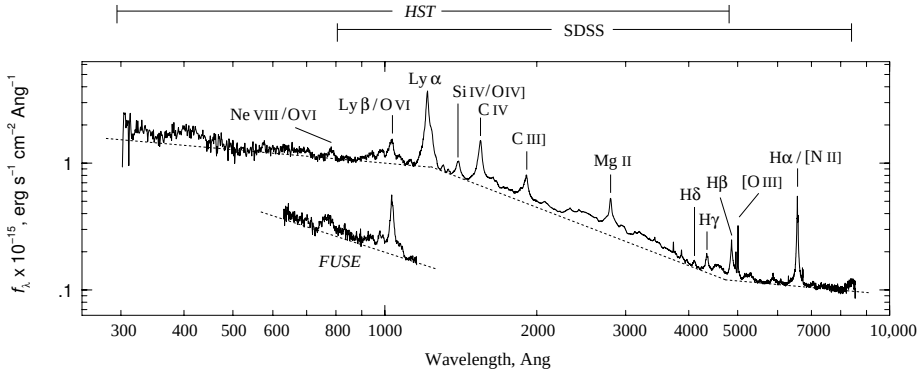


Figure 1.2: The composite quasar spectrum constructed by R. Telfer acquired with the *HST* (Telfer *et al.*, 2002) and SDSS facilities (Vanden Burk *et al.*, 2001). The *HST* data cover the wavelength range 291–4989 Å and the SDSS data cover the range 800–8554 Å. The lower spectrum (offset on the flux scale) is the composite quasar spectrum acquired with *FUSE* (Scott *et al.*, 2004), covering the rest–frame wavelength range 630–1156 Å [*HST*+SDSS composite spectrum obtained courtesy of R. Telfer. *FUSE* composite spectrum obtained from the Multi–mission Archive at STScI (MAST).]

## 1.3 Intrinisc absorbers

### 1.3.1 Narrow line absorbers (NALs)

Narrow absorption lines (NALs) are interpeted as high ionization outflow with velocities on the order of $\sim 1000$ [km sec$^{-1}$]. The are observed in roughly

Collect papers on ApJ page for Ganguly's paper.

NALs absorb the BELs **??**

NAL absorption seen in aborption against the BEL cloud on the opposite side of the conical funnel Hamman *et al.* (1993); **?**); **?**. (show in detailed figure of quasar structure).

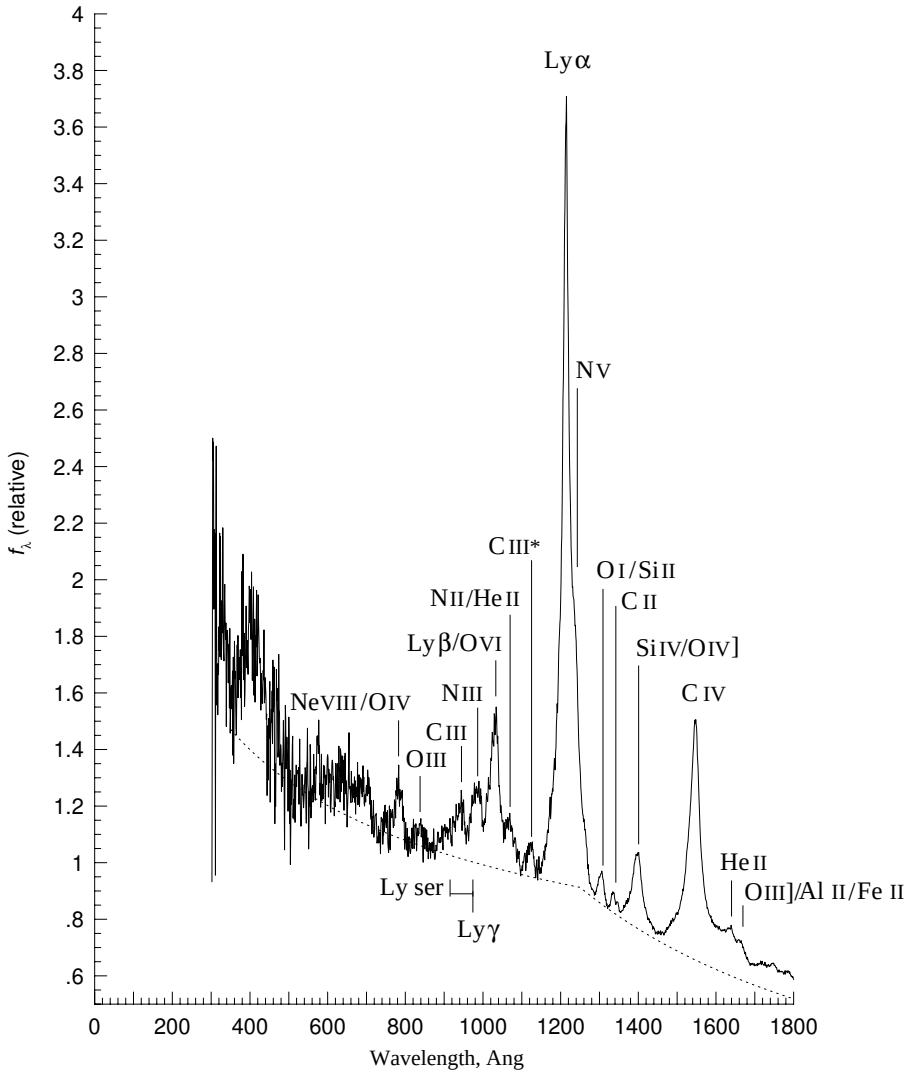


Figure 1.3: The composite quasar spectrum constructed by R. Telfer acquired with the *HST* (Telfer *et al.*, 2002) and SDSS facilities (Vanden Burk *et al.*, 2001). The *HST* data cover the wavelength range 291–4989 Å and the SDSS data cover the range 800–8554 Å. The lower spectrum (offset on the flux scale) is the composi te quasar spectrum acquired with *FUSE* (Scott *et al.*, 2004), covering the rest–frame wavelength range 630–1156 Å [*HST*+SDSS composite spectrum obtained courtesy of R. Telfer. *FUSE* composite spectrum obtained from NASA/ADS electronic database.]

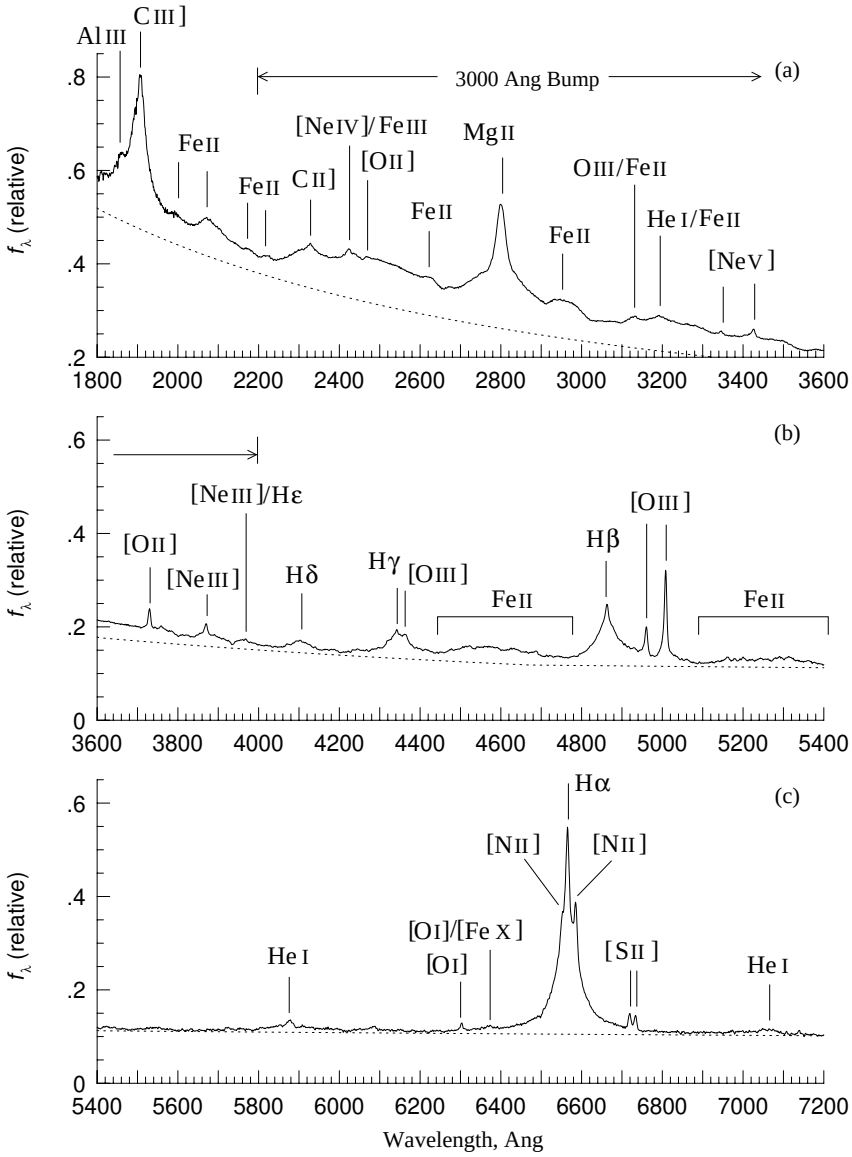


Figure 1.4: The composite quasar spectrum constructed by R. Telfer acquired with the *HST* (Telfer *et al.*, 2002) and SDSS facilities (Vanden Burk *et al.*, 2001). The *HST* data cover the wavelength range 291–4989 Å and the SDSS data cover the range 800–8554 Å. The lower spectrum (offset on the flux scale) is the composite quasar spectrum acquired with *FUSE* (Scott *et al.*, 2004), covering the rest–frame wavelength range 630–1156 Å [*HST*+SDSS composite spectrum obtained courtesy of R. Telfer. *FUSE* composite spectrum obtained from NASA/ADS electronic database.]

### 1.3.2 Broad line absorbers (BALs)

Broad absorption lines (BALs) in quasar spectra are almost universally interpreted as high velocity outflow and part of the quasar structure. The absorption is blueshifted relative to the emission lines of the same transition and can extend to velocities as great as 0.1–0.2$c$, or 30,000–60,000 [km sec$^{-1}$]. The population of BAL quasars are divided into two classes, high–ionization and low–ionization, defined by the presence of broad CIV $\lambda$1549 and MgII $\lambda$2800 asborption, repsectively. These are refered to as Hi–BALs and Lo–BALs, though broad CIV absorption is always present in lo–BAL quasars.

BALs and high–velocity outflows exceeding 10–20 times the velocity width of NALs, are observed in roughly 10–20% of the optically–selected quasar population[4]. From the SDSS DR3 quasi–stellar object catalog, Knigge *et al.* (2008) estimate that the fraction of BAL quasars is 17% with an upper limit of 23%. Xinyu, Shankar, & Svakoff (2008) reported 40% of 2MASS detected quasars are BAL quasars, and suggest this implies a substantial bias against optical selection of BAL quasars due to the presence of the broad absorption and high levels dust extinction. In fact, BAL quasars are reported to have redder spectral energy distributions and are likely to have higher bolometric luminosities compared to unabsorberd quasars (Ganguly *et al.*, 2007).

Virtually all radio–quiet quasars exhibit high–velocity outflows (Weymann *et al.*, 1991; Hamman *et al.*, 1993). The question is whether the converse is true: are all BAL quasars radio quiet? If so, this would suggest that the structure or structures giving rise to BALs are linked to quasar radio properties. Optical surveys of the early 1990s were suggestive of the affirmative (e.g., Stocke *et al.*, 1992), but the FIRST Bright Quasar Survey survey (FBQS) discovered a substantial number of radio–load BAL quasars (Becker *et al.*, 2000).

BAL quasars are found to be strong X–ray absorbers, which implies very large column densities on the order of $N$(HI) = few $\times$ $10^{23}$ [cm$^{-2}$] (Gallagher *et al.*, 2002; Fan *et al.*, 2009). Such large column densities are 2–3 orders of magnitude larger than inferred from ultraviolet and optical spectra. Fan *et al.* (2009) report a significant correlation between X–ray absorption and the maximum velocity of absorption, but do not find that HI column density correlates with BAL parameters in general (such as the balnicity index, see below).

The fact that BAL quasars comprise roughly 10–20% of the optically–selected quasar population, has been key observation for developing models of quasar structure. Two competing speculations are that the presence of BAL outflows in a quasar spectrum is due to (1) the orientation of the quasar structure as seen from the perspective of the observer (Weymann *et al.*, 1991; Cohen *et al.*, 1995; Goodrich & Miller, 1995; Hines & Wills, 1995; Murray & Chiang, 1995; Elvis, 2000), or to (2) the presence of winds during a relatively brief temporal period early in the quasar's evolution (Becker *et al.*, 2000; Gregg etal, 2000), when it is speculated to be in the process of emerging from an optically thick

[4]More precisely, 10–20% of optically–selected quasars are Hi–BAL quasars, whereas only 1% exhibit Lo–BAL features. However, Boroson & Meyers (1992) found that 10% of infrared–selected quasars are Lo–BAL quasars

dusty shroud of gas (Voit, Weymann, & Korista, 1993; Sanders *et al.*, 1988). In the orientation model, it is implied that roughly 10-20% of the solid angle of the structure would be high velocity outflowing wind material, whereas in the evolutionary model it is implied that the BAL phase lasts approximately 10–20% of the lifetime of the quasar.

For radio–loud BAL quasars, the orientation model is challenged by the large scatter in radio spectral indices (the presence of both flat and steep spectral energy distrobutions, Becker *et al.*, 2000), since these indices are believed to be good indicators of the quasar structure orientation (relative to the jets).

#### 1.3.2.1 The absorption and balnicity indices

The balnicity index (BI, also simply refered to as "the balnicity") was the first quantitative metric proposed and employed to define a BAL quasar (Weymann *et al.*, 1991), often refered to as a BALQSO in the literature. The absorption index, AI, was later introduced by Hall *et al.* (2002) to provide a more general metric for intrinsic and/or associated absorption. For the purpose of classifying BAL quasars from optical spectra, the BI and AI metrics are most commonly computed using the C IV $\lambda\lambda 1548, 1550$ doublet absorption blueward of the C IV $\lambda 1549$ emission line.

For computing balnicity, the centroid of the emission line is assigned a velocity of $v = 0$ [km sec$^{-1}$]. Applying the relativistic formula,

$$v = c\sqrt{\frac{1-(\lambda/\lambda_c)^2}{1+(\lambda/\lambda_c)^2}}, \tag{1.9}$$

where $\lambda_c$ is observed wavelength of the emission line centroid, the measured flux at wavelength $\lambda$ can be converted to the flux at velocity $v$. The BI metric is then defined as

$$\mathrm{BI} = -\int_{25{,}000}^{3000} C(v)\left\{1-\frac{f(v)}{0.9}\right\}dv, \tag{1.10}$$

where $f(v)$ is the normalized counts (or flux) in the spectrum as a function of velocity, and where BI and the limits of integration are in units of [km sec$^{-1}$]. The constant $C(v) = 0$ unless $f(v) < 0.9$ is satisfied without interuption over a continuous velocity window of 2000 [km sec$^{-1}$], in which case $C(v) = 1$ within the window. If the condition $f(v) > 0.9$ occurs the constant is reset to $C(v) = 0$. As the integrand is evaluated, it is possible that the value of $C(v)$ can be toggled several times.

Based upon Eq. 1.10, a quasar is classified as a BAL quasar if BI $> 0$ [km sec$^{-1}$]. The definition of BI ensures that BAL absorption is significant (at least 10% flux decrement), broad (a minimum of 2000 [km sec$^{-1}$]), and substantially blue shifted with respect to the quasar (minimum $v > 3000$ [km sec$^{-1}$]). This latter criterion is based upon the observation that BAL absorption is often "detatched", i.e., there is a significant velocity gap between the lowest velocity outflow of the absorption and the emission line centroid.

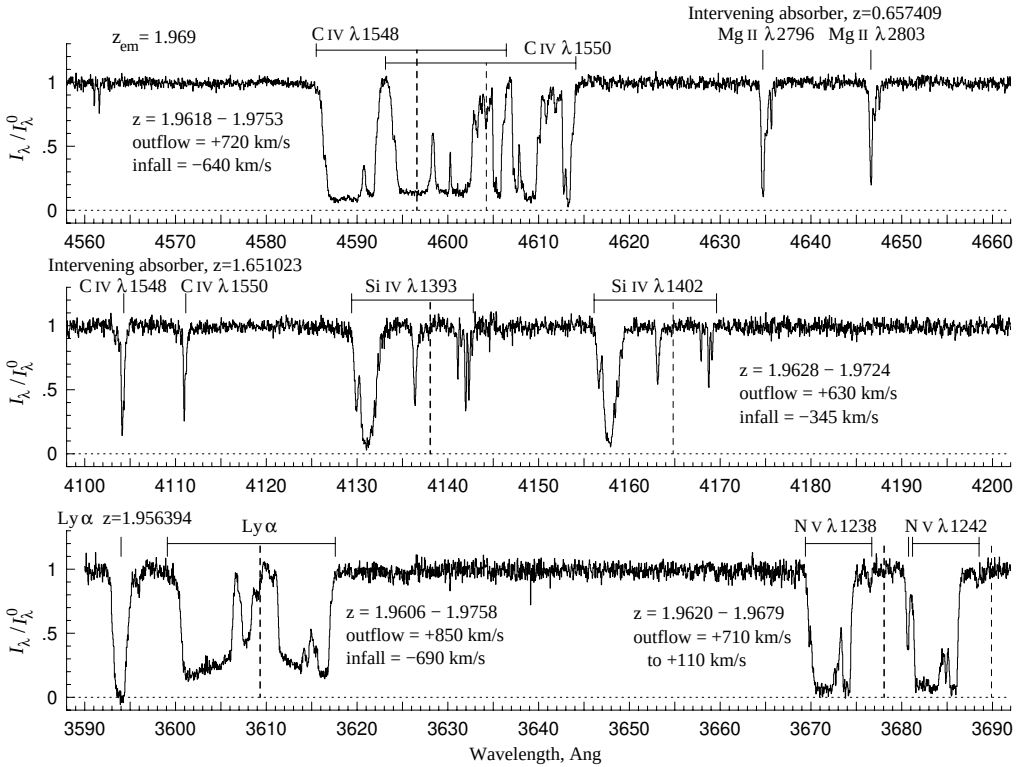


Figure 1.5: Segments of the continuum normalized spectrum of a redshift $z_{em} = 1.969$ quasar, focusing on the CIV $\lambda\lambda 1548, 1550$ (top panel), SiIV $\lambda\lambda 1393, 1402$ (center panel), and Ly$\alpha$+NV $\lambda\lambda 1238, 1242$ (lower) intrinsic absorption lines. For each featured absorption transition, a vertical dashed line marks the systemic redshift of the quasar and a horizontal bar provides the wavelength range of the absorption. The CIV $\lambda\lambda 1548, 1550$ and SiIV $\lambda\lambda 1393, 1402$ doublets, and the Ly$\alpha$ absorption exhbit both outflow (absorption blueward of systemic), and inflow (absorption redward of systemic), whereas NV absorption is seen only in outflow. Also shown are $z = 0.6574$ intervening MgII absorption and $z = 1.6510$ intervening CIV absorption. The square bottomed profile shapes with non–zero flux indicate that the absorbing material only partially covers the emitting source, and is one tall–tale sign that the absorption is intrinsic to the quasar. [Spectrum obtained with the Keck/HIRES facility, provided courtesy of W. Sargent.]

It has always been recognized that the definition of a BAL quasar employing the BI metric is somewhat arbitray; quasars with significant intrinisc absorption with velocities less than 3000 [km sec$^{-1}$] will have BI = 0, or quasars for which the widths of the absorption lines are less than 2000 [km sec$^{-1}$] will also have BI = 0 even if the outflow velocities achieve 10% of light speed. For this reason, the the absorption index, AI, has also been applied as a metric to identify BAL quasars. The definition of AI as applied to balnicity is (Trump *et al.*, 2006)

$$\mathrm{AI} = \int_0^{29{,}000} C(v)\,\{1 - f(v)\}\,dv, \tag{1.11}$$

where $f(v)$ is the normalized counts (or flux) in the spectrum as a function of velocity, and where, as with BI, AI and the integration limits are in units of [km sec$^{-1}$]. Note that the integral includes absorption right up to the centroid of the emission line. The constant $C(v) = 0$ except within 1000 [km sec$^{-1}$] velocity wide windows in which $f(v) < 0.9$ is satisfied, in which case $C(v) = 1$.

The main differences between BI and AI is that AI can be non–zero when BI = 0 for the conditions (1) all the absorption resides at velocities less than 3000 [km sec$^{-1}$], (2) all the absorption resides at velocities greater than 25,000 [km sec$^{-1}$], and/or (3) when multiple absorption features are present and one or more has a velocity width greater than 1000 [km sec$^{-1}$] but less than 2000 [km sec$^{-1}$].

A second difference is that, though the units for both BI and AI are [km sec$^{-1}$], the weighting factor $1 - f(v)/0.9$ employed for BI has no direct physical interpretation, where as the factor $1 - f(v)$ employed for AI results in AI being the summed equivalent width (in velocity units) of all absorption features having minimum widths of 1000 [km sec$^{-1}$] or greater. AI by its very definition is a more complete and intuitive metric than is BI for identifying broad absorption.

#### 1.3.2.2 Beyond AI and BI

The fraction of quasars that classify as BAL quasars is a key quantity for constraining models of quasar structure. There has been much debate in the literature with regard to the metrics and possible selection effects or hidden variables. Knigge *et al.* (2008) undertook a careful examination of AI and BI and report that the logarithm of the AI metric is a bimodel distribution with one peak at 500 [km sec$^{-1}$] and the second peak at 3000 [km sec$^{-1}$]. Quasars populating the narrower component of the distribution have BI = 0, whereas most, but not all of those populating the broader component have BI > 0, and would appear toidentify as BAL quasars. Thus, AI > 0 as a criterion for identifying a BAL quasar yeilds substantial overestimate in the fraction of BAL quasars.

Though Knigge *et al.* favor BI over AI for identifying BAL quasars in optical spectra, they find that BI underestimates the fraction of optically–selected BAL quasars. Focusing on the bimodalility of the AI distribution, Knigge *et al.* employed KMM decomposition, and focusing on the BI distribution, employed a Learning Vector Quantization (LVQ) method; both endeavors were undertaken to identify mis–classified BAL quasars.

KMM decomposition is a "mixture–modeling" algorithm based upon an "expectation maximization" algorithm. The AI data are fit with multiple Gaussian distributions, the number of which are user specified. The algorithm then calculates the Gaussian means and variances using maximum likelihood methods. The statistical significance of various components are then assessed. LVQ is a neural network learning algorithm. In this application, the network comprises to classes, BAL quasars and non–BAL quasars. Based upon a training set, quasars are classified by maximum similarity of their continuum normalized C IV absorption lines in the range $\lambda\lambda$1400–1700 Å.

The full explanation if these techniques are beyond the scope of this text. What is important is that the methods for identifying classes of quasars are becoming increasingly sophisticated; it is not clear if AI and BI will retain their utility as metrics for classifying BAL and non–BAL quasars.

## 1.4 A model of quasar structure

Models of quasar structure that invoke winds, the so–called wind models, have been favored since the mid–1990s

(Murray & Chiang, 1995) (Murray & Chiang, 1998)

Proga, Stone, & Kallman (2000) ??? check this ref (hydrodynamic model)

Ganguly *et al.* (2007) suggest radiative

BALs previous models- thought to be viewed edge on.

BEL Funnel wall width of 0.1 the funnel radius gives

**Intrinsic and associated absorption data**

- The emission line profile shapes suggest two kinematic components, a broad component with FWHM 5000 [km sec$^{-1}$] and a highly peaked narrow component of with FWHM 1000 [km sec$^{-1}$].
- The lack of absorption lines intrinsic to or associated with the quasar environment in roughly 40–45% of the quasar population.
- The presence of NAL absorption intrinisc to or associated with the quasar environment in roughly 40–45% of the quasar population.
- The presence of BAL absorption, or winds intrinisc to the quasar environment in roughly 10–20% of the quasar population.
- The fact that BAL quasars have emission lines and continuum spectal energy distributions that are statistically consistent with those of non–BAL quasars (Weymann *et al.*, 1991).

In both the NAL and BAL absorption, the profiles appear saturated over 50–80% of their velocity spreads in that they exhibit the smooth flat–bottomed shapes suggestive of zero transmission. However, there often is 5–20% transmitted flux in these saturated profiles. This suggests that NAL and BAL absorption does not fully occult the emission source(s). Furthermore, the residual flux in

these saturated profiles is polarized ata level of $\sim$ 10% in BAL profiles and $\sim$ 0.5% in NAL profiles. This suggests that the resdual flux is light into the line of sight.

**Trends with source luminosity**

- There is a trend between emission line equivalent width and quasar luminosity. The emission line equivalent widths are smaller for quasars with higher luminosities and are larger for quasars with lower luminosities. This is known as the Baldwin effect (Baldwin, 1977), and is especially pronounced in high ionization emission lines.

- The presence of NALs is common in low luminosity quasars and in Seyfert galaxies, but rarer in high luminosity quasars.

Time variability ; Partial covering

In Figure 1.6, the structural model for quasars proposed by Elvis (2000) is presented.

## 1.5 Intervening absorbers

### 1.5.1 HI–selected absorbers

#### 1.5.1.1 The Lya forest

#### 1.5.1.2 The Lyman limit systems (LLS)

#### 1.5.1.3 The damped Ly$\alpha$ systems (DLA)

The Ly$\alpha$ forest is illustrated in Figure 1.7. In this spectral region captures only the Ly$\alpha$ transition of neutral hydrogen, so each absorption line provides a 1:1 correspondence with the line of sight distribution of Ly$\alpha$ cloud.

Two Lyman limit systems (LLS) are illustrated in Figure 1.8. The feature of the ionization limit is known as the Lyman limit break, or Lyman break.

Two damped Ly$\alpha$ systems (DLAs) are illustrated in Figure 1.10. The feature of the ionization limit is known as the Lyman limit break, or Lyman break.

Two damped Ly$\alpha$ systems (DLAs) are illustrated in Figure 1.11. The feature of the ionization limit is known as the Lyman limit break, or Lyman break.

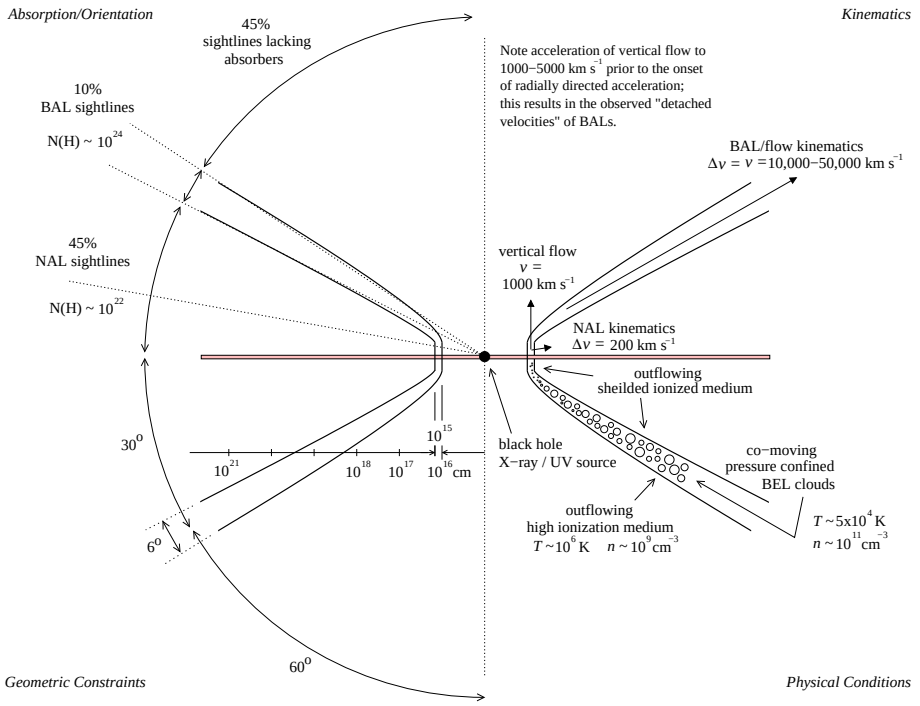


Figure 1.6: Edge–on schematic of the structure of a quasar as proposed by Elvis (2000). A vertical wind flows off a narrow region of a rotating accretion disk. The flow is then propelled and accelerated radially outward via radiation pressure to velocities on the order of $0.1c$. Embedded in the wind $T \simeq 10^6$ K wind are cooler, higher density, pressure confined clouds. The model provides a single structure designed to explain a wide range of observed characteristics of quasars as a population. As explained in the text, each quadrant of the figure highlights a set of characteristics, physical and phenomonological (Figure adapted from Elvis, 2000)

## 1.5.2 Metal–line selected systems

### 1.5.2.1 OVI absorbers

### 1.5.2.2 CIV absorbers

### 1.5.2.3 MgII absorbers

### 1.5.2.4 CaII absorbers

---

# References

Baker, J. C., & Hunstead, R. W. 1995, Revealing the effects of orientation in composite quasar spectra, *Ap. J.*, **425**, 95

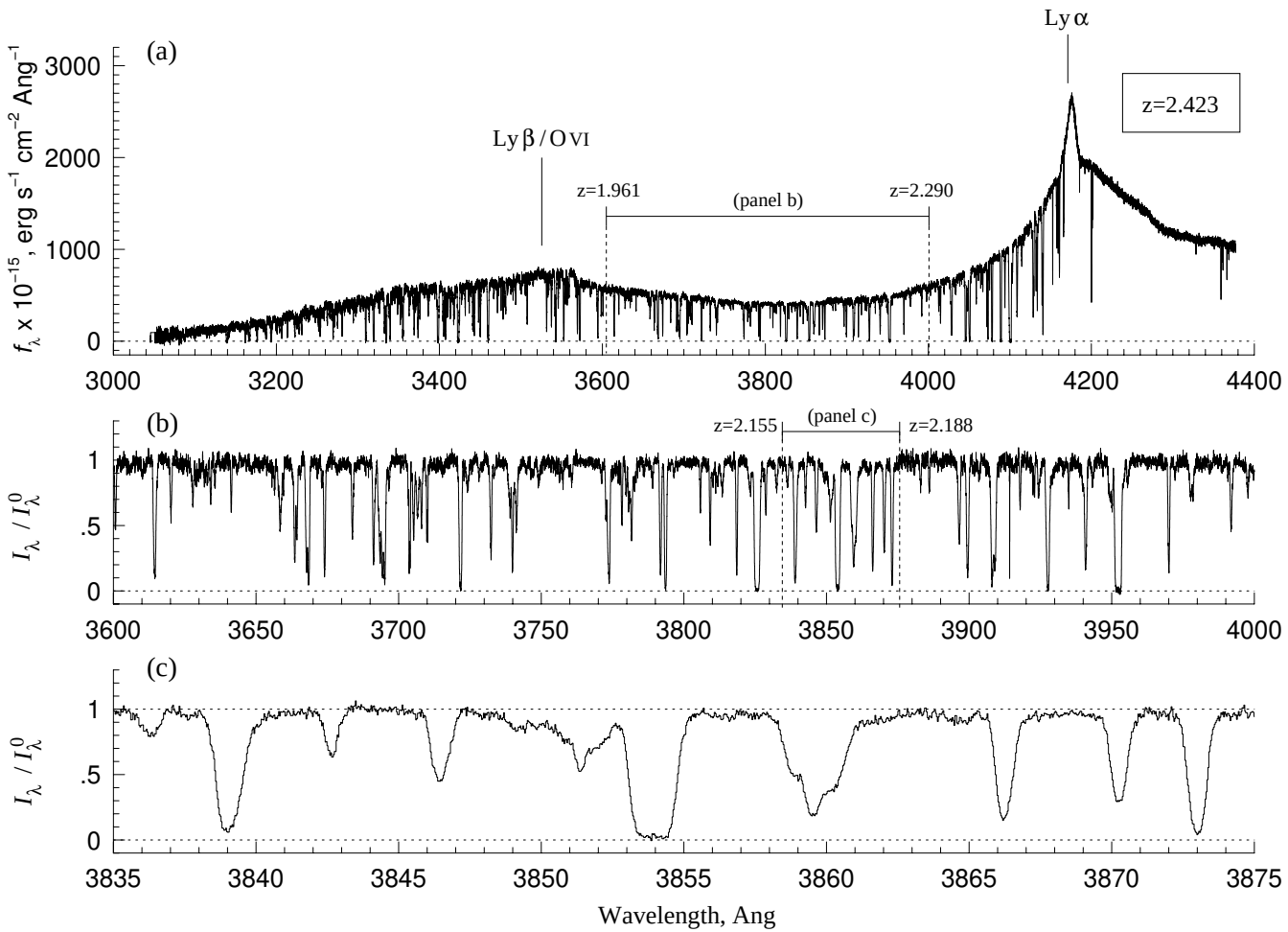


Figure 1.7: (*a*) Spectrum of a redshift $z_{em} = 2.423$ quasar covering 920–1285 Å in the quasar rest frame, emphasizing the spectral region dominated by Ly$\alpha$ forest absorption. (*b*) The relative flux, $I_\lambda/I^0_\lambda$, over the observed spectral range 3600–4000 Å, as marked in panel *a*, corresponding to the redshift range $1.961 \leq z \leq 2.290$ for cosmologcally intervening Ly$\alpha$ absorption. (*c*) An expanded view of the relative flux covering the observed spectral range 3835–3875 Å, as marked in panel *b*, detailing the complexity of the neutral hydrogen optical depth to Ly$\alpha$ photons over the redshift range $2.155 \leq z \leq 2.188$. At these wavelengths, the spectral resolution is FWHM = 0.085 Å, which spans three pixels. [Spectrum obtained with the VLT/UVES facility, acquired from the ESO VLT archive, courtesy of M. Murphy and the UVES Squad collaboration.]

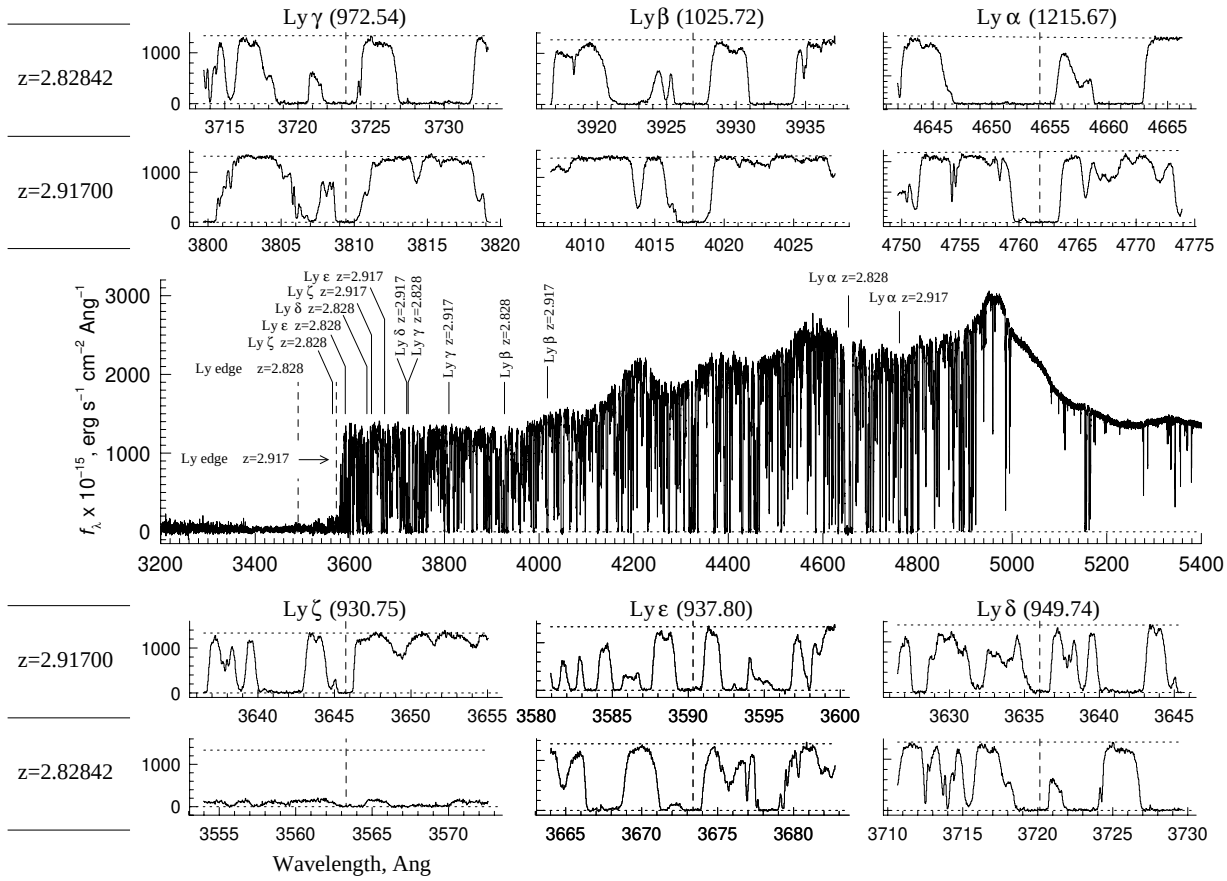


Figure 1.8: (*center*) Spectrum of a redshift $z_{em} = 3.054$ quasar covering 790–1330 Å in the quasar rest frame, capturing Ly$\alpha$ forest absorption (the Ly$\alpha$ emission line of the quasar peaks at $\simeq$ 4960 Å). Two of the Ly$\alpha$ absorption lines are identified as Lyman limit systems, at $z = 2.91700$ (4761.8 Å) and $z = 2.82842$ (4654.1 Å). The first six transitions of the Lyman series, i.e., Ly$\alpha$, Ly$\beta$, Ly$\gamma$, Ly$\delta$, Ly$\epsilon$, and Ly$\zeta$, and the ionization edge are labeled. The onset of the dramatic flux decrement, or break, in the observed flux at $\simeq$ 3570 Å (slightly redward of the vertical dotted line labeled "Ly edge $z = 2.917''$) is due to the blended absorption of higher order transitions in the Lyman series. (*detail*) The individual Lyman series transitions as labeled. The wavelength range for each panel covers a redshift range $\Delta z = \pm 0.01$ centered about the system redshift (marked by the vertical dashed lines. [Spectrum obtained with the VLT/UVES facility, acquired from the ESO VLT archive, courtesy of M. Murphy and the UVES Squad collaboration.]

Baldwin, J. A. 1975, Spectrophotometry of low–redshift quasi–stellar objects, *Ap. J.*, **201**, 26

Baldwin, J. A. 1977, Luminosity indicators in the spectra of quasi–stellar objects, *Ap. J.*, **214**, 679

Becker, R. H., *et al.* 2001, The FIRST Bright Quasar Survey – III. the south Galactic cap, *Ap. J. Supp.*, **135**, 227

Becker, R. H, White, R. L., Gregg, M. D., Brotherton, M. S., Laurent–Muehlheisen, S. A., & Arav, N 2000, Properties of radio–selected broad absorption–line quasars from the FIRST Bright Quasar Survey, *Ap. J.*, **538**, 72

Boroson, T. A., & Meyers, K. A., 1992, The optical properties of IR–selected and Mg II broad absorption lines quasars, *Ap. J.*, **397**, 442

Boyle, B. J., A composite QSO spectrum, *M.N.R.A.S.*, **243**, 231

Brotherton, M. S., Tran, H. D., Becker, R. H., Gregg, M. D., Laurent–Muehleisen, S. A., & White, R. L. 2001, Composite spectra from the FIRST Bright Quasar Survey, *Ap. J.*, **546**, 775

Brotherton, M. S., Wills, B. J., Francis, P. J., & Steidel, C. C. 1994, The intermediate line region of QSOs, *Ap. J.*, **430**, 495

Chan, Y.–W. T., & Burbidge, E. M. 1975, Emission–line strengths and the chemical compsitions of quasi–stellar objects, *Ap. J.*, **198**, 45

Cohen, M. H., Ogle, P. M., Tran, H. D., Vermeulen, R. C., Miller, J. S., Goodrich, R. W., Martel, A. R. 1995, Spectropolarimetry of two broad absorption line quasars with the W. M. Keck telescope, *Ap. J. Lett.*, **448**, 77

Cristiani, S. & Vio, R. 1990, The composite spectrum of quasars, *Astron. & Astroph.*, **227**, 385

Croom, S. M., Rhook, K., Corbett, E. A., Boyle, B. J., Netzer, H., Loaring, N. S., Miller, L., Outram, P. J., Shanks, T., & Smith, R. J. 2002, The correlation of line strength with luminosity and redshift from composite quasi–stellar object spectra, *M.N.R.A.S.*, **337**, 275

Davidson, K. 1972, Photoionization and the emission–line spectra of quasi–stellar objects, *Ap. J.*, **171**, 213

Elvis, M. 2000, A structure for quasars, *Ap. J.*, **545**, 63

Fan, L. L., Wang, H. Y., Wang, T., Wang, J., Dong, X., Zhang, K., & Cheng, F. 2009, The correlation between X–ray and UV properties of BAL QSOs, *Ap. J.*, **690**, 1006

Forster, K., Green, P. J., Aldcroft, T. L., Vestergaard, M., Foltz, C. B., & Hewett, P. C. 2001, Emission line properties of the Large Bright Quasar Survey, *Ap. J. Supp.*, **134**, 35

Francis, P. J., Hewett, P. C., Foltz, C. B., Chaffee, F. H., Weymann, R. J., & Morris, S. L. *Ap. J.*, **373**, 465

Francis, P. J., Hooper, E. J., & Impey, C. D. 1993, The ultraviolet spectra of radio–loud and radio–quiet quasars, *A. J.*, **106**, 417

Gallagher, S. C., Brandt, W. N., Chartas, G. & Garmire, G. P. 2002, X–ray spectroscopy of quasi–stellar objects with broad ultraviolet absorption lines, *Ap. J.*, **567**, 37

Ganguly, R., Brotherton, M. S., Cales, S., Scoggins, B., Shang, Z., & Vestergaard, M. 2007, Outflows and the physical properties of quasars, *Ap. J.*, **665**, 990

Green, P. J. 1998, *Ap. J.*, **498**, 170

Gregg, M. D., Becker, R. H., Brotherton, M. S., Laurent–Muehleisen, S. A., Lacy, M., & White, R. L. 2000, Discovery of a FR–II broad absorption line quasar from the FIRST survey, *Ap. J.*, **544**, 142

Goodrich, R. W., & Miller, J. S., 1995, Polarization clues to the structure of broad absorption line quasi–stellar objects, *Ap. J.*, **448**, 73

Hall, P. B., *et al.* 2002, Unusual broad absorption line quasars from the Sloan Digital Sky Survey, *Ap. J. Supp.*, **141**, 267

Hamman, F., Korista, K. T., & Morris, S. L. 1993, On the geometry, covering factor, and scattering emission properties of QSO broad absorption line regions, *Ap. J.*, **415**, 541

Hines, B. H., & Wills, B. J. 1995, The polarized spectrum of the FeII–rich broad absorption line QSO IRAS 07598+6508, *Ap. J. Lett.*, **448**, 69

Knigge, C., Scaringi, S., Goad, M. R., & Cottis, C. E. 2008, The intrinsic fraction of broad–absorption line quasars, *M.N.R.A.S.*, **386**, 1426

Malhotra, S. 1997, Detection of the 2175 Å dust feature in MgII asorption systems, *Ap. J. Lett.*, **488**, 101

McIntosh, D. H, Rix, H.–W., Rieke, M. J., & Foltz, C. B. 1999, Redshifted and blueshifted broad lines in luminous quasars, *Ap. J. Lett.*, **517**, 73

Murray, N., & Chiang, J. 1995, Active galactic nuclei disk winds, absorption lines, amd warm absorbers, *Ap. J. Lett.*, **454**, 105

Murray, N., & Chiang, J. 1998, Photoionization of disk winds, *Ap. J.*, **494**, 125

Oke, J. B. 1966, Photoelectric spectrophotometry of quasi–stellar sources, *Ap. J.*, **145**, 668

. Oke, J. B., Neugebauer, G., & Becklin, E. E. 1970, Absolute spectral energy distributions of quasi–stellar objects from 0.3–2.2 microns, *Ap. J.*, **159**, 341

Sanders, D. B., Soifer B. T., Elias, J. H., Neugbauer, G., & Mathews, K. 1988, Warm luminous galaxies in the IRAS survey– the transition from galaxy to quasar?, *Ap. J. Lett.*, **328**, 35

Schmidt, M., & Green, R. F. 1983, Quasar evolution derived from the Palomar bright quasar survey and other complete surveys, *Ap. J.*, **269**, 352

Scott, J. E., Kriss, G. A., Brotherton, M., Green, R. F., Hutchings, J., Shull, J. M., & Zheng, W. 2004, A composite extreme–ultraviolet QSO spectrum form *FUSE*, *Ap. J.*, **615**, 135

Stocke, J. S., Morris, S. L., Weymann, R. J., & Foltz, C. B. 1992, The radio properties of the broad–absorption–line QSOs, *Ap. J.*, **396**, 487

Telfer, R. C., Zheng, W., Kriss, G. A., & Davidson, A. F. 2002, The rest–frame extreme–ultraviolet spectral properties of quasi–stellar objects, *Ap. J.*, **565**, 773

Trump, J. R., *et al.* 2006, A catalog of broad absorption line quasars from the Sloan Digial Sky Survey third data release, *Ap. J. Supp.*, **373**, 23

Vanden Berk, D. E., *et al.* 2001, Composite quasar spectra from the Sloan Digital Sky Survey, *A. J.*, **122**, 549

Voit, G. M., Weymann, R. J., & Korista K. T. 1993, Low–ionization broad absorption lines in quasars, *Ap. J.*, **413**, 95

Wampler, E. J. 1967, Scanner observations of four quasi–stellar radio sources, *Ap. J.*, **147**, 1

Weymann, R. J., Morris, S. L., Foltz, C. B., & Hewitt, P. C. 1991, Comparison of the emission–line and continuum properties of broad absorption line and normal quasi–stellar objects, *Ap. J.*, **373**, 23

Xinyu, D., Shankar, F., & Svakoff, G. R. 2008, 2MASS reveals a large intrinisc fraction of BALQSOs, *Ap. J.*, **672**, 108

Zheng, W., Kriss, G. A., Telfer, R. C., Grimes, J. P., & Davidson, A. F. 1997, A composite *HST* spectrum of quasars, *Ap. J.*, **475**, 469

Table 1.1: Ultraviolet/Optical Composite Quasar Spectra

| Reference | Survey | $N_{\rm QSO}$ | Subsamples | $\lambda$ [Å] |
|---|---|---|---|---|
| Davidson (1972) | | 11 | | |
| Chan & Burbidge (1975) | | 160 | | |
| Boyle (1990) | AAO | 402 | | 1075–3550 |
| Cristiani & Vio (1990) | HQS | 60 | RQ/RL | 1000–8000 |
| Francis *et al.* (1991) | LBQS | 718 | | 800–5800 |
| Weymann *et al.* (1991) | LBQS | 71 | BAL | 800–3100 |
| Francis *et al.* (1993) | LBQS | 255 | RQ/RL | 800–5800 |
| Brotherton *et al.* (1994) | CIT/ALS | 15 | ILR/VBLR | 1100–2000 |
| | LBQS | 200 | ILR/VBLR | 1175–2000 |
| Baker & Hunstead (1995) | MQS | 60 | $R_{\rm CL}$ | 1000–7000 |
| Malhotra (1997) | CIT | 92 | Mg II abs | 1950–3600 |
| Zheng *et al.* (2002) | *HST* | 101 | RQ/RL | 350–3000 |
| Green (1998) | LBQS | 124 | XF/XB | 2200–5200 |
| | *IUE* | 48 | XF/XB | 1000–1700 |
| Brotherton *et al.* (2001) | FBQS | 657 | RQ/RL/BAL | 900–7500 |
| Vanden Burk *et al.* (2001) | SDSS | 2204 | | 800–8555 |
| Croom *et al.* (2002) | 2dF | 21,102 | | 980–6800 |
| | 2dF+6dF | 200[a] | $\Delta z$, $\Delta M_B$ | 980–6800 |
| Telfer *et al.* (2002) | *HST* | 184 | RQ/RL | 350–3000 |
| Scott *et al.* (2004) | *FUSE* | 85 | $\Delta z$, $L_{1100}$ | 630–1155 |

[a] Mean number per subsample drawn from 21,102 spectra.

Notes. — *Survey Acronyms:* AAO = Anglo Australian Observatory; ALS = CIT + heterogeneous data; CIT = Caltech optical survey; HQS = Hamburg/European Southern Observatory Quasar Survey; FBQS = FIRST Bright Quasar survey; LBQS = Large Bright Quasar Survey; MQS = 408 MHz Molongo Quasar Sample; SDSS = Sload Digital Sky Survey; *Subsample Acronyms:* BAL = broad absorption line; ILR = intermediate line region; $L_{1100}$ = luminosity at $\lambda$1100; Mg II abs = aligned in rest frame of Mg II absorbers; $R_{\rm CL}$ = ratio of core to lobe flux density; RQ = radio quiet; RL = radio loud; VBLR = very broad line region; XF = X–ray faint; XB = X–ray bright (see references for details).

Table 1.2: Composite Quasar Emission Line Features[a]

| $\lambda_{obs}$ | ID | $\lambda_{obs}$ | ID | $\lambda_{obs}$ | ID |
|---|---|---|---|---|---|
| 782.6 | NeVIII 774.60 | 1856.7 | AlIII 1857.40 | 3425.7 | [NeV] 3426.84 |
| | OIV 789.32 | 1906.0 | CIII] 1908.73 | 3729.7 | [OII] 3728.48 |
| 838.3 | OIII 832.93 | 1991.8 | FeII UV 50 | 3869.8 | [NeIII] 3869.85 |
| 944.4 | CIII 977.02 | 2076.6 | FeII UV 48 | 3968.4 | [NeIII] 3968.58 |
| 984.4 | NIII 990.02 | 2175.6 | FeII UV 79 | | H$\epsilon$ 3971.20 |
| 1033.0 | Ly$\beta$ 1025.72 | | FeII UV 370 | 4102.7 | H$\delta$ 4102.89 |
| | OVI 1033.83 | 2222.3 | FeII UV 118 | 4346.4 | H$\gamma$ 4341.68 |
| 1066.1 | NII 1083.99 | | FeII UV 376 | 4363.9 | [OIII] 4364.44 |
| | HeII 1084.94 | 2327.3 | CII] 2326.44 | 4853.1 | H$\beta$ 4862.68 |
| 1121.7 | CIII* 1175.71 | 2423.5 | [NeIV] 2423.83 | 4960.4 | [OIII] 4960.30 |
| 1216.3 | Ly$\alpha$ 1215.67 | | FeIII UV 47 | 5008.2 | [OIII] 5008.24 |
| 1239.9 | NV 1240.14 | 2468.0 | [OII] 2471.03 | 5877.4 | HeI 5877.29 |
| 1305.4 | OI 1304.35 | | FeII UV 395 | 6303.1 | OI] 6302.05 |
| | SiII 1306.82 | 2626.9 | FeII UV 1 | 6370.5 | OI] 6365.54 |
| 1336.6 | CII 1335.30 | 2800.3 | MgII 2798.75 | | [FeX] 6376.30 |
| 1398.3 | SiIV 1396.76 | 2964.3 | FeII UV 78 | 6551.1 | NII 6549.85 |
| | OIV] 1402.06 | 3127.7 | OIII 3133.70 | 6564.9 | H$\alpha$ 6564.61 |
| 1546.2 | CIV 1549.06 | | FeII Opt 82 | 6585.6 | NII 6585.28 |
| 1637.8 | HeII 1640.42 | 3191.8 | HeI 3188.67 | 6718.9 | [SII] 6718.29 |
| 1664.7 | OIII] 1663.48 | | FeII Opt 6 | 6733.7 | [SII] 6732.67 |
| | AlII 1670.79 | | FeII Opt 7 | 7056.7 | HeI 7076.20 |
| | FeII UV 40 | 3345.4 | [NeV] 3346.82 | | |

[a] IDs obtained from Vanden Burk *et al.* (2001), Telfer *et al.* (2002), and Scott *et al.* (2004)

Table 1.3: Unified Quasar Model

| Abs Class | Observed Frequency | Viewing Angle [degrees] | $\Delta v$ Abs [km sec$^{-1}$] | $v$ Gas [km sec$^{-1}$] | Dynamics |
|---|---|---|---|---|---|
| NAL | 10% | 0–30° | 100–200 | 1000 | vertical |
| BAL | 45% | 27–33° | $10–50 \times 10^3$ | $10–50 \times 10^3$ | radial |
| no–abs | 45% | 30–90° | ... | ... | |

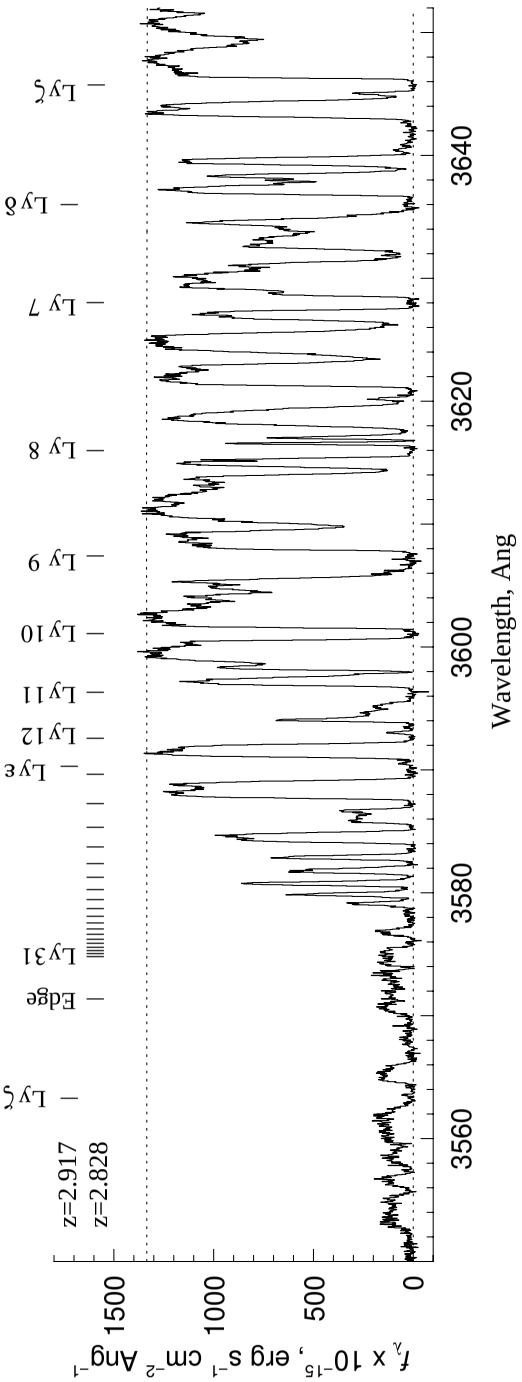


Figure 1.9: An expanded view of the Lyman edge from the $z = 2.91700$ and $z = 2.82842$ Lyman limit systems shown in Figure 1.8. Ticks label the higher order Lyman series lines (upper row $z = 2.82842$, lower row $z = 2.91700$ to the 31st line in the series). It is clear that several absorption lines, mostly Ly$\alpha$ lines at lower redshifts, are blended with the Ly$\alpha$ series lines in this complex spectral region. Also, note that the dramatic flux decrement occurs redward of the ionization edge due to the blending of the higher series lines of the Lyman limit system. [Spectrum obtained with the VLT/UVES facility, acquired from the ESO VLT archive, courtesy of M. Murphy and the UVES Squad collaboration.]

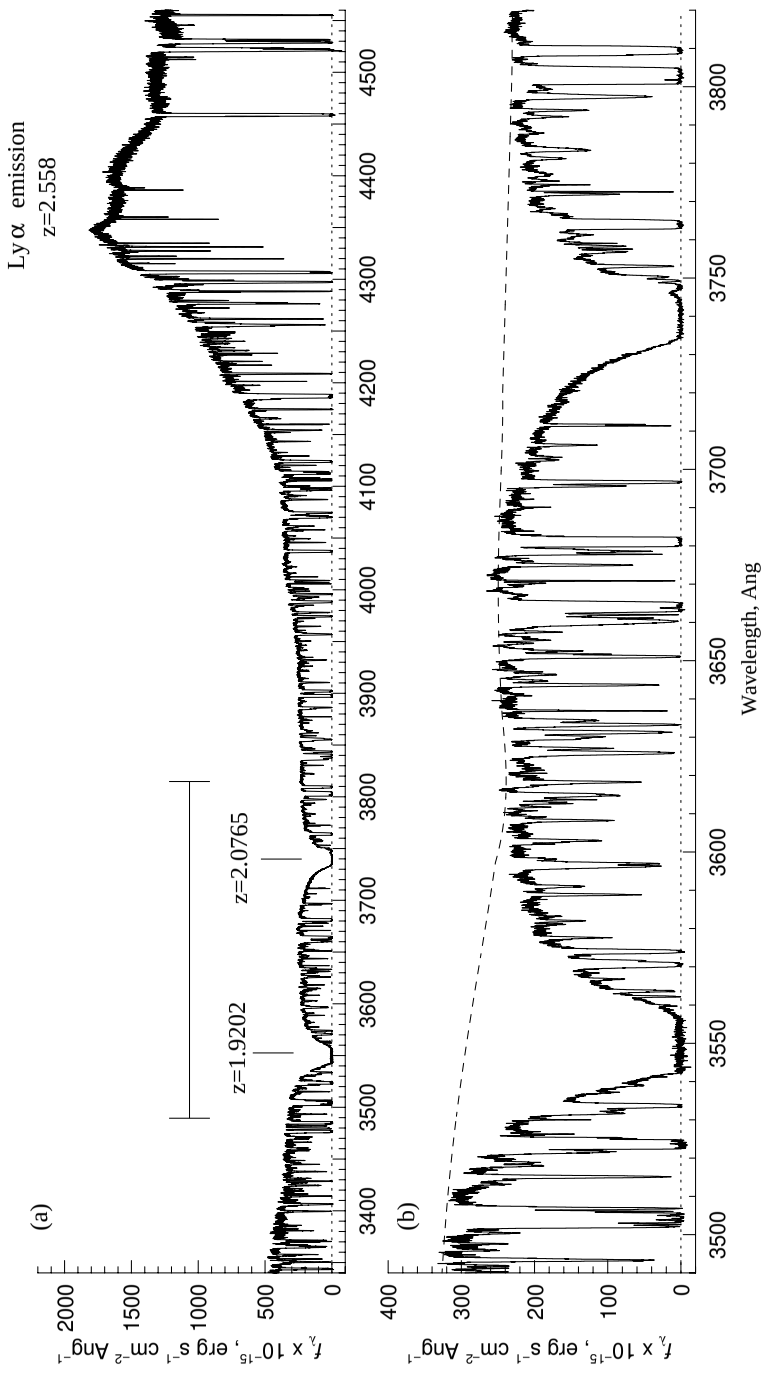


Figure 1.10: (*a*) The spectrum of redshift $z_{em} = 2.558$ quasar covering a portion of the Ly$\alpha$ forest. Intervening to the quasar are two damped Ly$\alpha$ absorbers (DLAs) at $z = 2.0765$ and $z = 1.9202$. (*b*) An expanded view of the two DLAs, including an estimate of the continuum flux of the quasar, shown as a dashed curve. The tall–tale signature of a DLA is the broad curved damping wings. Note that DLAs are always intermixed with Ly$\alpha$ forest absorbers, and since DLA profiles are so broad, it is common for Ly$\alpha$ absorbers to populate the wings (the blue wing of the $z = 2.0765$ DLA is a nice exception). [Spectrum obtained with the VLT/UVES facility, acquired from the ESO VLT archive, courtesy of M. Murphy and the UVES Squad collaboration.]

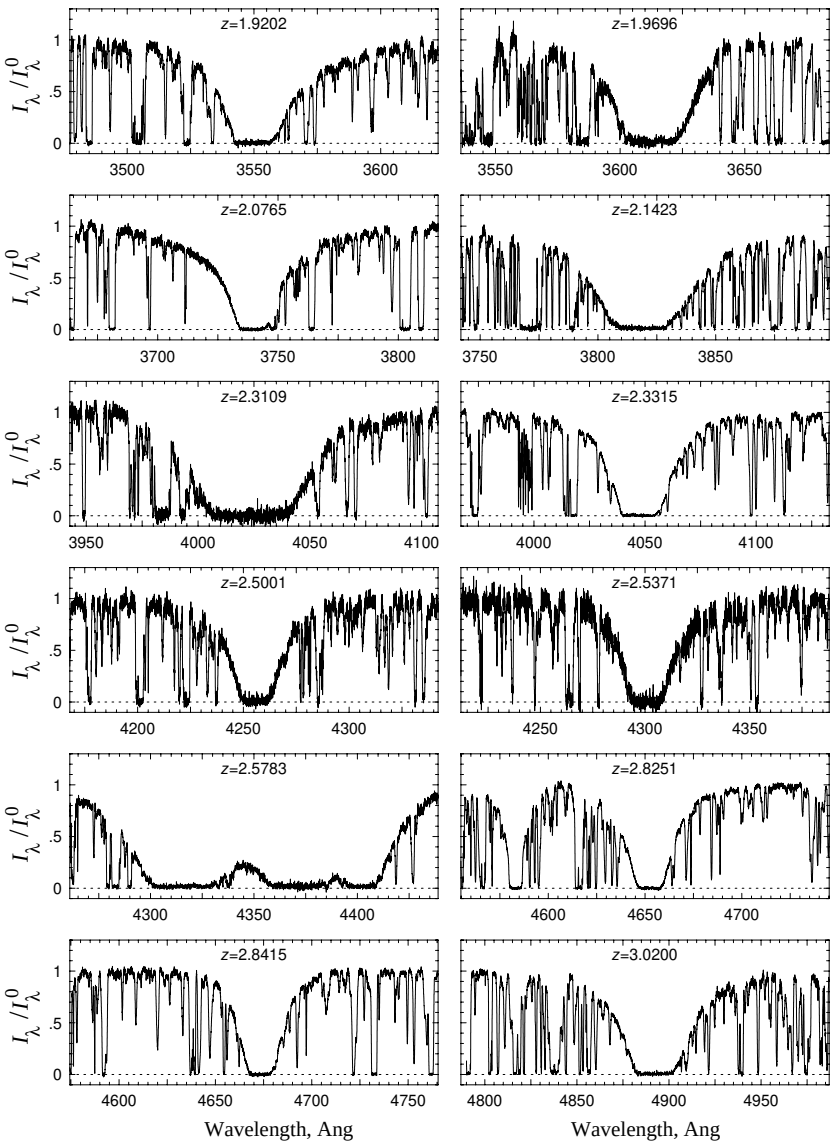


Figure 1.11: Examples of damped Ly$\alpha$ absorption profiles (in relative flux units) presented in increasing redshift order. Note the heavy blending with Ly$\alpha$ forest clouds, some of which are Lyman limit systems. [Spectra obtained with the HIRES/Keck and VLT/UVES facilities, the former provided courtesy of W. Sargent and the latter acquired from the ESO VLT archive, courtesy of M. Murphy and the UVES Squad collaboration.]